Semidilute and Concentrated Polymer Solutions near Attractive Walls: Dynamic Monte Carlo Simulation of Density and Pressure Profiles of a Coarse-Grained Model

Ras B. Pandey,[†] Andrey Milchev,[‡] and Kurt Binder*

Institut für Physik, Johannes Gutenberg Universität Mainz, D-55099 Mainz, Staudinger Weg 7, Germany

Received September 10, 1996; Revised Manuscript Received November 25, 1996[⊗]

ABSTRACT: Using a bead−spring model of flexible polymer chains, we study polymer adsorption from solutions onto attractive planar walls, varying both the strength of the adsorption potential ϵ and the concentration of the solution over a wide range. Treating the case of good solvents, the profiles of density and pressure are computed and it is shown that thermal equilibrium between the adsorbed layer and the bulk solution is obtained. The case of a wall with purely repulsive potential under otherwise identical conditions is treated for comparison. It is shown that for the strongly adsorbing wall there is a pronounced layering, while a layered structure at the repulsive wall occurs only for high concentrations, and this layering is also much weaker. These features carry over to the profile of the total pressure as well. From the difference in the pressure components in the parallel and perpendicular directions we compute also the interfacial energy between the polymer film and the repulsive wall as a function of the bulk density in the film. We use a dynamic Monte Carlo method which yields a Rouse behavior for the chain length N that is used, $N = 32$. The time-dependent mean-square displacements parallel and perpendicular to the wall are studied, and relaxation times are extracted. For the considered conditions, the polymer films stay in the fluid phase and a glass-like freezing-in into nonequilibrium states does not occur.

1. Introduction

Thin polymeric films have important applications (protective coatings, adhesives, lubricants, etc.) and pose many challenging scientific problems.[1−12] There is an interesting interplay between bulk and surface properties in the interfacial regions between the bulk of the film and the adsorbing substrate on one side and the polymer solution (or air, respectively) on the other side of the film. A flexible polymer chain experiences a loss of configurational entropy near a wall but this may be outweighed by enthalpic gains due to wall−monomer interactions. The resulting changes in chain configurations are expected to influence also the dynamic behavior of these adsorbed polymer chains. Since chains which are partially adsorbed to the wall and mutually entangled are very hard to treat by analytical methods, only rather few papers deal with the theoretical aspects of the motion of chains in adsorbed layers,[13] and this problem is not so well understood yet. It is also hard to study experimentally, since the extent to which these layers are in thermal equilibrium is rather uncertain.[10,14] One may argue that as an adsorbed layer is formed by bringing a wall that is initially free of adsorbed polymers in contact with a polymer solution, the chains that get adsorbed first form many contacts with the wall and are irreversibly adsorbed, while chains coming later to the wall find much less adsorption sites available, and so the layer is in a state of incomplete equilibrium that reflects the history according to which the adsorbed film was prepared.[14] Theoretical treatments, on the other hand, typically use concepts that imply thermal equilibrium.

In this situation computer simulation is useful, since the conditions of the simulation can be chosen such that full equilibrium is established, and one can test the theoretical concepts more stringently than by the experiment. Also it is possible to deal with ideal and perfectly flat surfaces, very suitable to test the general mechanisms alluded to above, and disregard in a first step all the complications that real substrate surfaces have (corrugation on the atomistic scale, roughness on the mesoscopic scale, surface steps, adsorbed impurities, etc.). Of course, it may be desirable to add such complications one by one at a later stage, but this will not be considered here.

There have been numerous previous simulations of polymers near walls.[15−44] However, a large part of this work did address static properties only, while we are specifically interested in the interplay between static and dynamic properties. This interplay has occasionally been considered both for wall effects on melts[15,28,38] and solutions[44] and for the adsorption of single chains,[40] but a study where both the concentration of the polymer solution and the strength of the adsorption potential have been varied over a wide range has been lacking.

In the present work we consider a coarse-grained description on scales that are distinctly larger than the scales needed for a fully chemically realistic description of atomistic detail. Although an atomistically detailed simulation might seem attractive because of its potential to establish a link between physical properties and chemical structure, this is not feasible in our case because of the large length scales and time scales involved.[45−48] While one can study chemically realistic models of oligomers at interfaces,[24,32−34] we quote Leontidis et al.[48] to state that "we still have not reached the stage where realistically long polymeric chains with atomistic detail can be treated successfully". However, coarse-grained models of the type used here have yielded much useful insight for a lot of other problems already,[46,47] and we think that they are useful for a study of adsorbed polymer layers, too.

In section 2 we recall the model (whose bulk properties have been studied extensively in earlier work[49−51]).

[†] Present and permanent address: Department of Physics and Astronomy, The University of Southern Mississippi, Hattiesburg, MS 39405-5046.

[‡] Present and permanent address: Institute of Physical Chemistry, Bulgarian Academy of Sciences, 1113 Sofia, Bulgaria.

[⊗] Abstract published in *Advance ACS Abstracts,* January 15, 1997.

S0024-9297(96)01342-3 CCC: $14.00

Section 3 considers density and pressure profiles of the adsorbed films for a variety of conditions and also interfacial tensions are obtained. Section 4 presents some results on dynamic properties, while section 5 contains our conclusions.

2. Model and Simulation Geometry

The polymer chains are described by N "effective monomers" ($N = 32$ here) connected by springs representing "effective bonds", using the FENE (finitely extensible nonlinear elastic) potential for the bond length l,

$$U_{\mathrm{FENE}}(l) = -\frac{1}{2}K(l_{\max} - l_0)^2 \ln[1 - (l - l_0)^2/(l_{\max} - l_0)^2] \quad (1)$$

This potential has its minimum $U_{\mathrm{FENE}}(l_0) = 0$ for a bond length l_0, is harmonic in its vicinity, K being the associated spring constant $\{U_{\mathrm{FENE}}(l \approx l_0) \approx {}^1/_2K(l - l_0)^2\}$, but diverges logarithmically both for $l \to l_{\max}$ and $l \to l_{\min} = 2l_0 - l_{\max}$. Thus the length of the effective bond is restricted to the range $l_{\min} < l < l_{\max}$. We choose our unit of length such that $l_{\max} = 1$ and the other parameters are[49,51]

$$l_{\min} = 0.4, \qquad l_0 = 0.7, \qquad \frac{1}{2}K/k_{\mathrm{B}}T = 20 \quad (2)$$

The coarse-grained chains are treated as being fully flexible, and thus neither bond angle nor torsional potentials are included. Such a choice is reasonable, because one has the picture that groups of n successive chemical bonds along the backbone of the chain are combined into one effective bond such that the length of the effective bond is of the order of the persistence length[47] (typically hence $n \approx 5-10$). For these effective bonds the bond angle and torsional potentials that act on the level of chemical bonds must be clearly washed out. Of course, depending on the detailed conformation of the group of the n chemical bonds, the effective bond can be longer or shorter, and this variation is qualitatively represented by eq 1. The parameters of this potential (eq 2) are not chosen in order to optimize the mapping to any real polymer,[47] however, but rather for the sake of computational efficiency.

As a nonbonded interaction between effective monomers both of the same chain and of different chains, a Morse potential of strength ϵ_{M} is used,[49]

$$U_{\mathrm{M}}(r)/\epsilon_{\mathrm{M}} = \exp[-2\alpha(r - r_{\min})] - 2\exp[-\alpha(r - r_{\min})] \quad (3)$$

choosing the position $r_{\min}$ where this potential has its minimum of depth $-\epsilon_{\mathrm{M}}$ as $r_{\min} = 0.8$; i.e., the preferred distance between neighboring nonbonded ones ($r_{\min}$) is not the same as the preferred distance between neighboring bonded ones (l_0). In this way, a tendency to crystallization in dense configurations at low temperatures is avoided, and under these conditions the model gets rather trapped in glassy states,[52] as real polymers do. The parameter α describing the inverse range of this potential is chosen very large, $\alpha = 24$. This has the (desirable) consequence that the potential is extremely short ranged, $U_{\mathrm{M}}(r \geq 1) \approx 0$, which allows us to use very fast link-cell algorithms with a cell size of unity.[49,50] Choosing $\epsilon_{\mathrm{M}} = 1$ (and units of temperature such that $k_{\mathrm{B}} = 1$), it is known that the theta temperature for this model occurs at[51] $\Theta \approx 0.62$. In the present study, we work with a single choice of temperature in the good solvent regime, $T = 1$. The behavior of our model chains in dilute solution in the bulk has been characterized in detail in previous work,[49,51] which showed that the model is rather close to the asymptotic behavior that very long chains should exhibit in a good solvent; namely, the mean-square gyration radius $\langle R_{\mathrm{g}}^2 \rangle$ scales with chain length as $\langle R_{\mathrm{g}}^2 \rangle \propto N^{2\nu}$, with[53] $\nu \approx 0.59$. The fact that the present model is well tested and that its properties in the bulk are well studied and characterized (including also the concentration and chain length dependence[49,51]) is a further argument in favor of the choice of this model.

Dynamics is associated to the model by choosing a single monomer random hopping motion that is straightforward to implement in the framework of a Monte Carlo algorithm.[47] The attempted Monte Carlo update consists in a monomer displacement, where the new position is $\vec{X}' = \vec{X} + \Delta\vec{X}$, with $\Delta\vec{X} = (\Delta x, \Delta y, \Delta z)$ being chosen randomly and uniformly from the intervals $-0.5 \leq \Delta x, \Delta y, \Delta z \leq +0.5$. The potentials described above ensure that no intersection of bonds can occur; i.e., entanglement constraints are obeyed automatically and need not be enforced by extra (time-consuming!) constraints. The above displacement widths ensure a reasonably high acceptance rate A of the moves (A is of the order of 20%), and even for dense melts at $T > \Theta$ one has $A > 5$ %, and thus the rate of approach to equilibrium is still reasonable. Again it is stressed that the somewhat arbitrary choice of some of the parameters of the model is motivated to yield a reasonably fast performance of the algorithm. About 10^5 attempted updates of monomeric units occur per CPU second on IBM 6000 RISC workstations that were used for this investigation.

As expected, for single chains this algorithm yields a dynamics compatible with the Rouse model.[54] One must be aware, of course, that dynamic Monte Carlo methods yield purely diffusive and/or relaxational behavior,[47] the hydrodynamic backflow interaction is completely missing, and thus the Zimm model behavior[54] appropriate for dilute polymer solutions is not reproduced. In dense adsorbed layers at walls hydrodynamic forces are presumably screened out to a wide extent, and for the dynamic behavior of monomers inside such dense layers the neglect of hydrodynamic forces is probably irrelevant. This is not so for monomers belonging to the dilute or semidilute solution outside of the adsorbed layer, and hence one has to be careful when one tries to relate our model calculation to real systems. However, for many topics in the theory of polymer dynamics,[54] it was crucial to analyze the behavior in the pure Rouse limit first, and in this spirit the present work should be a useful first step.

As a simulation geometry we choose an $L \times L \times D$ box with $L = 32$, $D = 8$, and two impenetrable walls of area $L \times L$ at $z = 0$ and $z = D$, while in the x and y directions periodic boundary conditions are applied. At the left wall, a short-range attractive potential acts (in related work[40] the sign of ϵ was defined the opposite way)

$$U_{\mathrm{w}}(z) = \epsilon\{\exp(-2\alpha z) - 2\exp(-\alpha z)\} \quad (4)$$

The strength ϵ of this potential, which decays to zero over a distance δ of order 0.2, will be used as a control parameter; i.e., choices $\epsilon = 0$ (no adsorption), $\epsilon = +2$, $+4$, and $+8$ will be mostly considered. In previous work[40] on the adsorption of single chains, a slightly

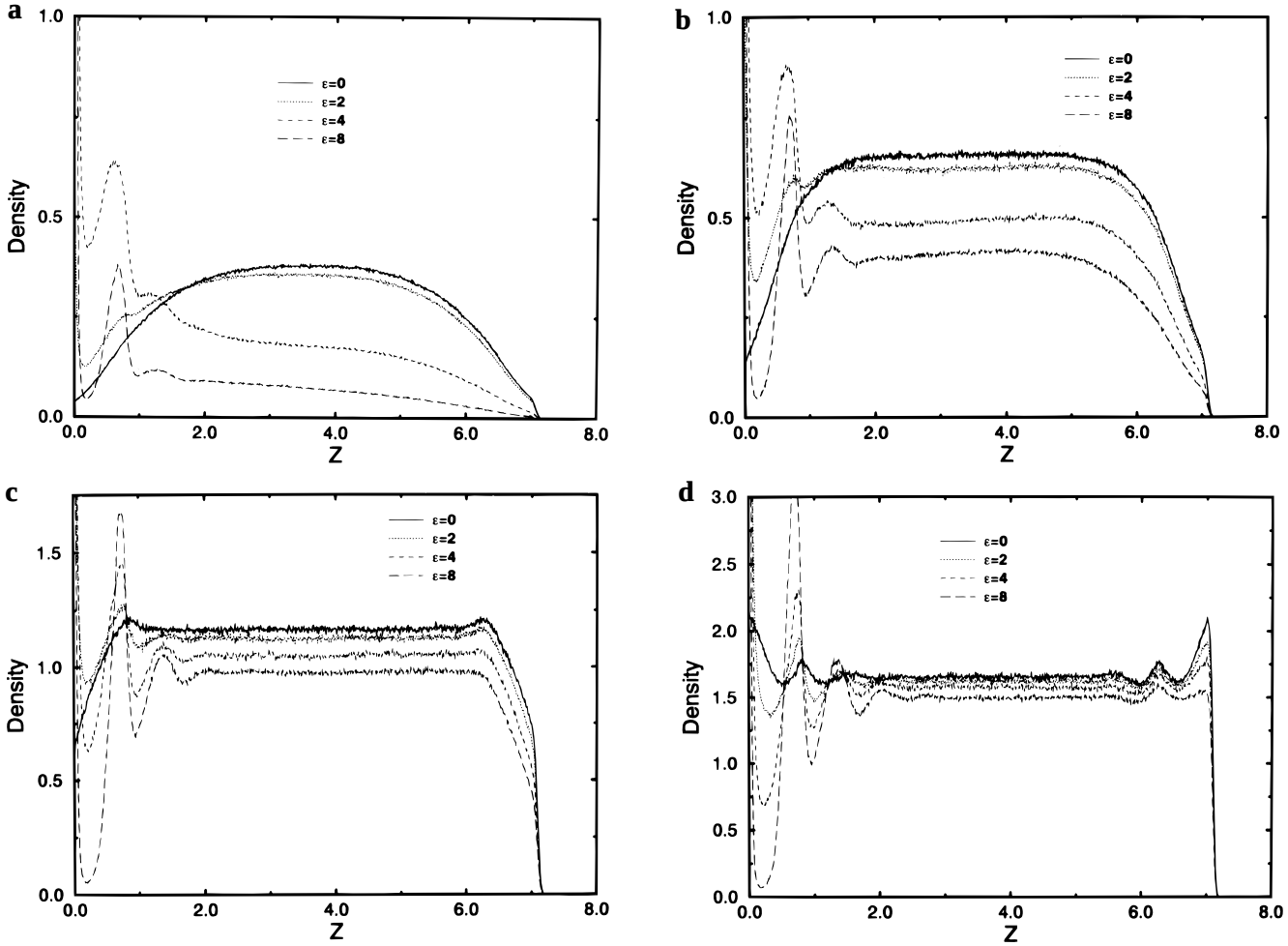

Figure 1. Density profiles $\rho(z)$ versus z for $\phi = 0.25$ (a), 0.50 (b), 1.0 (c), and 1.5 (d). Four choices of ϵ are included as shown.

different potential was used, namely a square well potential $U_{sw}(z) = \epsilon' < 0$ for $z < \delta' = 1/8$, $U_{sw}(z > \delta') = 0$. It was shown that dilute solutions in semi-infinite geometry exhibit an adsorption transition, where a single chain changes its conformation from a three-dimensional "mushroom" to a quasi-two-dimensional "pancake" attached to the surface[9,55,56] at

$$(\epsilon'/k_B T)_{ads} = -1.90 \pm 0.05 \qquad (5)$$

For the present choice of potential, however, the precise location of the adsorption transition for single chains is not yet known. We decided to abandon the potential of ref 40 in the present work and replace it by the smooth potential, eq 4, to avoid possible artifacts in the calculation of the pressure from the virial theorem, where one needs to take derivatives of the potential. But we think that for eq 4 the adsorption transition of single chains will also occur at a value of ϵ close to 2, since the half-width of the potential is not very different from the range δ' of the square well potential. Thus our range of ϵ for single chains (remember the choice $k_B T = 1$ used here) corresponds to the range from weak to very strong adsorption. Note that we can vary the adsorption strength $\epsilon/k_B T$ and the energy parameter of the Morse potential $\epsilon_M/k_B T$ (which controls the quality of the polymer solution in the bulk) as independent control parameters, unlike experiments for real systems where no arbitrary variation of several such parameters usually is feasible.

Our model differs from cases typically considered in the literature[1−12] in one basic aspect, however: this is the strictly short range of the adsorption potential, eq 4. The typical situation considered is a long-range van der Waals attraction, $U_w(z) \propto z^{-3}$. Of course, this van der Waals attraction is certainly no longer valid when one comes very close to the surface (say, the distance of a chemical bond), and it is likely that on this very short length scale much stronger chemical forces than the weak van der Waals attraction act. Note that the range of our potential is about one-sixth of the length of an effective bond in our model, and can hence be taken as representing such direct chemical interactions. Note also that the range δ is of comparable size as the width of the attractive part of the Morse potential, eq 3, which also represents such chemical forces, while the repulsive part of that potential (which steeply rises for $r < r_0$ where $r_0 = r_{min} - \ln 2/\alpha \approx 0.771$) represents the excluded volume of the n chemical groups that contribute to one effective monomer. Thus we think that our grossly simplified choices of potentials are nevertheless qualitatively physically reasonable and mutually consistent with each other.

At the other wall at $z = D$ we use a purely repulsive potential which we take of the shifted Lennard-Jones type. Defining $z' = D - z$, this potential is

$$U_{RW}(z') = \epsilon'[(z'/\sigma)^{-12} - 2(z'/\sigma)^{-6} + 1], \qquad z' < \sigma \qquad (6a)$$

$$U_{RW}(z') = 0, \qquad z' > \sigma \qquad (6b)$$

taking the range parameter $\sigma = 1$.

This second repulsive wall serves only to confine the polymer chains in the solution, and it should perturb

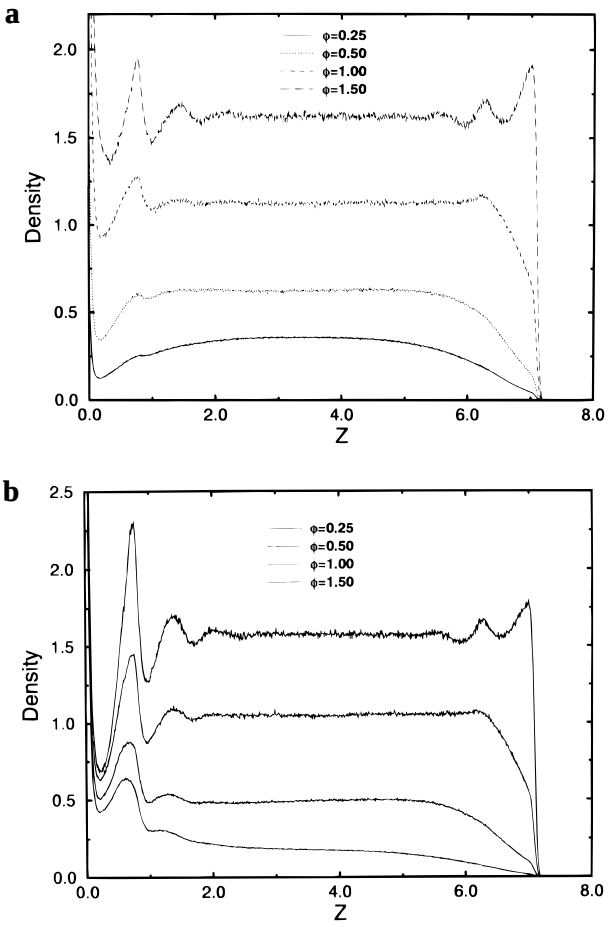

Figure 2. Density profiles $\rho(z)$ versus z for $\epsilon = 2$ (a), and $\epsilon = 4$ (b). Four choices of ϕ are included as shown.

the structure of the solution as little as possible. Choosing a smooth confinement potential rather than the simpler hard core interaction with the confining wall should damp out the density oscillations that one finds in dense systems confined near walls, and facilitates computation of the pressure from the virial theorem.

In some of our previous work,[42,43] we have rather used two equivalent attractive walls with the same potential, eq 4, both near $z = 0$ and near $z = D$. This choice has the disadvantage, however, that not precisely the same number of polymer chains gets adsorbed on both walls: the left wall may have $\eta/2 + \Delta\eta$ adsorbed chains and the right wall $\eta/2 - \Delta\eta$ chains, for a strongly adsorbing case where all chains get adsorbed that are initially in solution. This fluctuation $\Delta\eta$ is of the order $\eta^{1/2}$ and hence negligible in the thermodynamic limit, but not for our choice of a small simulation box. In principle, if one waits very long, one should see that the system equilibrates fully by chains that desorb from one wall and adsorb on the other such that the time average of $\Delta\eta$ is zero, but in practice these asymmetric configurations are perfectly metastable. This problem would complicate the analysis of the results.

As a further control parameter, we have used the overall monomer density $\phi = N\eta/(L^2D)$ in the system, studying the range from semidilute solution to melt densities ($\phi = 0.25$, 0.5, 1.0, 1.5); i.e., our simulation box contains from 64 chains (for $\phi = 0.25$) to 384 chains (for $\phi = 1.5$). Note, however, that due to the different local densities near the two walls the density of the bulk solution in the center of the thin film may differ appreciably from this average density. This happens particularly for the case of strong adsorption potential

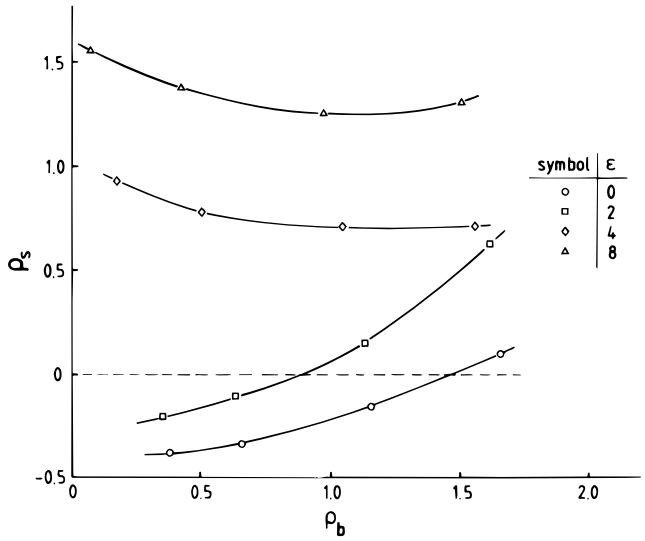

Figure 3. Surface excess plotted versus density in the bulk. Four choices of ϵ are shown.

and not too high average density. As an initial state, we always prepared a system with zero adsorption potential, for which the chains are distributed rather homogeneously throughout the film (apart from the region close to the repusilve wall at $z = D$). When the adsorption potential is switched on, one has to relax the system a long time (typically of the order of 10^6 or 10^7 Monte Carlo steps (MCS) per monomer), since chains need to diffuse from the bulk of the film to the adsorbing wall. Therefore the question whether thermal equilibrium has been established needs very careful consideration. In fact, the slowness of this diffusion process has forced us to work with this relatively small value of the thickness D.

3. Density Profiles, Pressure Profiles, and Surface Tension

(a) Density and Pressure Profiles of the Adsorbed Films. For the calculation of the density profile, we divided the distance D into 1024 bins and sampled how many monomers fall into each bin. We normalized the profiles such that

$$\int_0^D \rho(z)\, dz/D = \phi \tag{7}$$

These results are shown in Figures 1 and 2. It is seen that for $\phi = 0.25$ a flat behavior in the center of the film is reached only for $\epsilon = 0$ and $\epsilon = 2$, but not for the larger values of ϵ. This inhomogeneity of the thin polymer film is a consequence of the low value of the bulk density in these cases. We estimate the bulk density of the solution from the average around the center of the film

$$\rho_b = \int_{3.5}^{4.5} \rho(z)\, dz \tag{8}$$

Of course, eq 8 makes sense only if all density variations induced by the walls have decayed near the center of the film. One expects that for semidilute solutions this decay of density inhomogeneities is controlled also by the screening length ξ_b of excluded volume interactions in the bulk,[53]

$$\xi_b = \xi_{b0}\rho_b^{-\nu/(3\nu-1)} \approx \xi_{b0}\rho_b^{-0.77}, \qquad \rho_b \to 0 \tag{9}$$

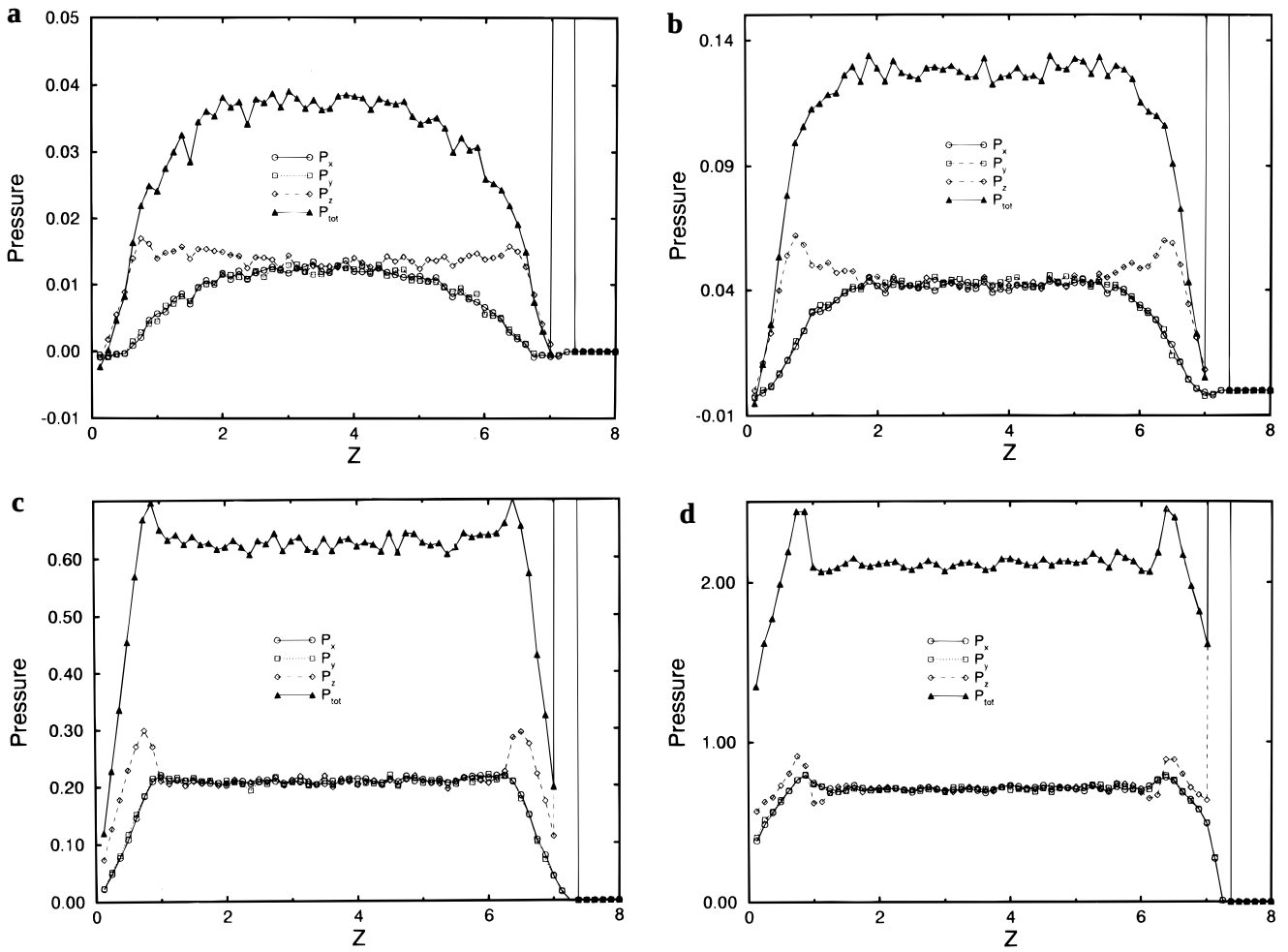

Figure 4. Profiles of the diagonal components of the pressure tensor and of the total pressure for a nonadsorbing wall ($\epsilon = 0$) (and four choices of ϕ: $\phi = 0.25$ (a), $\phi = 0.50$ (b), $\phi = 1.0$ (c), and $\phi = 1.5$ (d).

where $\nu \approx 0.59$ was used. This screening length has been estimated in independent work[57] for our model, and it was found that eq 9 is a reasonable description of our data over a wide density range (up to $\rho \approx 1$), with $\xi_{b0} \approx 1.4$. However, when we fit our density variation near the repulsive wall by a phenomenological expression $\rho_b - \rho(z) \approx \rho_b \exp[-(z' - z_0)/\xi]$, where $z_0 \approx 7.2$ is the value where $\rho(z)$ vanishes (cf. Figure 1), we find a significantly smaller decay length ξ than ξ_b as given in eq 9, although the density dependence of ξ is similar to that of ξ_b. Therefore we feel that our film thickness of $D = 8$ is indeed large enough to study the equilibrium between the adsorbed layer and the polymer solution confined in the center of the film.

Density profiles are seen to rise steeply within the range δ of our adsorption potential. A pronounced minimum occurs near $z \approx 0.2-0.3$, which is followed by a peak at $z \approx 0.7$. This peak results from effective monomers which are nearest neighbors along the chain of monomers that are in the bound part of the adsorbed layer ($z < \delta$). While for $\phi = 0.25$ a second layer peak due to monomers that are still further out can only be recognized as a weak shoulder, for higher densities this second layer peak in the profile gets more pronounced. For the highest density studied ($\phi = 1.5$) and large adsorption potentials ($\epsilon \geq 4$) there is even clear evidence for a third layering peak, and also a layering structure at the repulsive wall at the other side of the film develops (Figure 1d).

However, one must be aware that the layering structure that develops near the two walls does depend on the details of our model—neither heights nor the wavelength of these density oscillations is supposed to have any universal character. In fact, for real polymers one should expect that the density oscillations that develop actually reflect the packing of the actual monomers, and hence do not occur on the scale of coarse-grained bonds but on the scale of chemical bonds. Also the chain stiffness, size and shape of the monomers, possible side groups, etc. play an important role for these packing effects near hard walls. These expectations find confirmation from simulations of realistic models of very short chains.[15,32-34] Therefore the present model is useful only as a qualitative guidance, but not in its quantitative detail.

A useful characteristic of the adsorption is the total amount that is adsorbed on the surface. We define this surface excess from the density profile as

$$\rho_s = \int_0^{D/2} [\rho(z) - \rho_b] \, dz \tag{10}$$

Figure 3 shows a plot of ρ_s versus ρ_b. It is seen that for small ρ_b and not too large ϵ ($\phi \leq 0.5$, $\epsilon \leq 2$) ρ_s actually is negative: the entropic repulsion of the hard wall at $z = 0$ is not sufficiently overcome by the adsorption potential to produce a net adsorption. Interestingly, for $\epsilon = 2$ the sign of ρ_s changes near $\rho = 1$; i.e., the entropic repulsion of the hard wall is the less efficient the denser the system. For strong adsorption potential ($\epsilon \geq 4$), the trend is different, however: ρ_s somewhat decreases with increasing density ρ_b. The reason for this behavior is

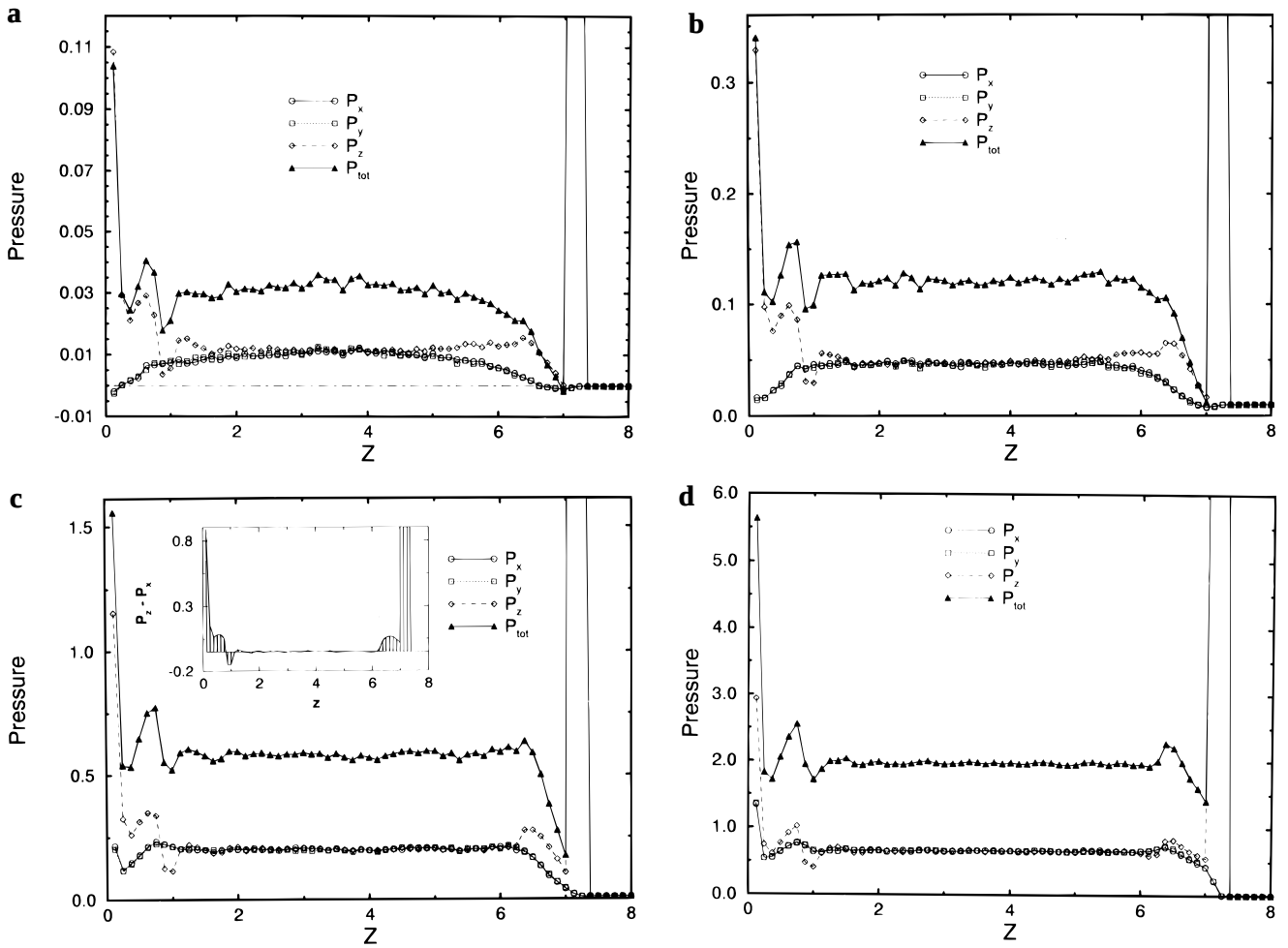

Figure 5. Same as Figure 4 but for a weakly adsorbing wall ($\epsilon = 2$). Insert in (c) shows the difference between P_z and P_x to show that isotropic behavior in the bulk of the film is nicely obtained.

that for such a strongly adsorbing wall a high-density monolayer of monomers in direct contact with wall ($z < \delta$) forms. The density in this monolayer is not much affected by ρ_b. Thus the contribution to the integral eq 10 from this tightly bound layer decreases with increasing ρ_s. Only for rather dense systems ($\rho_b \geq 1$) this decrease due to the first layer becomes compensated by some extra density accommodated in the further layers, and ρ_s becomes nearly independent of ρ_b.

In all cases, however, is the surface excess of order one—a thick absorbed layer hence is not formed in these good solvent conditions. We believe that this conclusion is of general validity, and not specific to our particular coarse-grained model.

We next turn to the behavior of the pressure, which we have obtained from the virial theorem.[58] Since our system is anisotropic (directions parallel and perpendicular to the walls are not equivalent) and inhomogeneous, it makes sense to consider a local pressure tensor $p_{\alpha\beta}(z)$ which depends on the distance z from the adsorbing wall. This pressure tensor is defined by ($\alpha, \beta = x,y,z$, $\vec{r}_{ij} = \vec{r}_i - \vec{r}_j$)

$$p_{\alpha\beta}(z) = \rho(z) k_B T \delta_{\alpha\beta} - \frac{1}{6V} \sum_{i \neq j} (\vec{r}_{ij})_\alpha \frac{\partial U(\vec{r}_{ij})}{\partial (\vec{r}_{ij})_\beta} \times [\delta(z_i - z) + \delta(z_j - z)] \quad (11)$$

Here $U(\vec{r}_{ij})$ is the sum of all potentials defined in eqs 1−4. To simplify the notation we abbreviate the diagonal components of the pressure tensor as $P_x = p_{xx}$, $P_y = p_{yy}$, $P_z = p_{zz}$ and also define a "total pressure" $P_{tot} = P_x + P_y + P_z$. For symmetry reasons, we expect $P_x = P_y$, of course, and this symmetry does hold with good accuracy for our data (Figures 4−6). We see that generally the total pressure follows the density profile—regions of high density correspond to regions of high pressure. We also note that the pressure gives a good criterion for the judgment of whether bulk behavior is reached, because in the bulk the system must be fully isotropic: $P_x = P_y = P_z$. We see that for $\epsilon = 0$ and $\phi = 0.25$ we just reach bulk behavior right in the center of the film (Figure 4a), while for $\epsilon = 4$, $\phi = 0.25$ the curve for P_z seems to intersect the curve for $P_x = P_y$ under a finite angle (Figure 6a), and thus a flat region, where irrespective of the precise value of z all three components agree, is not reached. Thus the analysis of the pressure profiles is of great help to establish whether the desired goal of the present investigation, namely the study of the full equilibrium of the adsorbed surface layer with adjacent polymer solution, actually has been reached.

It is also of interest to compare the structure of the pressure profile with the density profiles in more detail. One immediately notes that the pronounced density minimum that occurs close to the wall (for $z \approx 0.2$−0.3) does not correspond to a similarly pronounced minimum in the pressure profile—typically the pressure in this minimum is not much less than the bulk pressure. Also it is interesting to note that for $\epsilon = 0$, where the density varies monotonically near the wall, the pressure component P_z exhibits a peak whose position coincides with

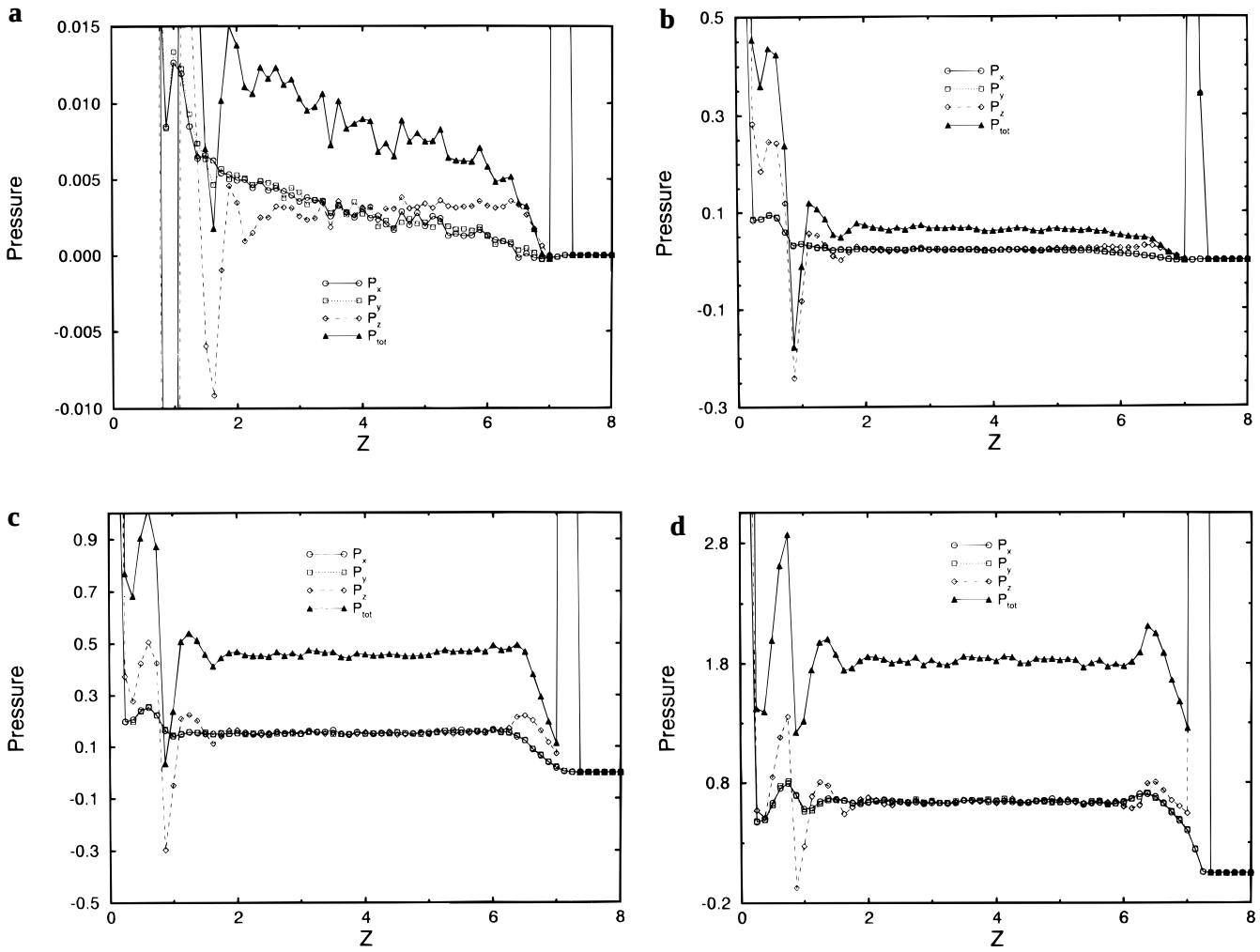

Figure 6. Same as Figures 4 and 5 but for a strongly adsorbing wall ($\epsilon = 4$).

the position of the maximum of the density profile.

In Figure 6b one can note a small region near $z = 1$ where the total pressure is negative. Presumably this is an indication that the system is not yet fully equilibrated in this case, and chains are still attracted from the bulk to the surface region.

We analyze where the different contributions to the pressure tensor come from (Figure 7). It is seen (for the example shown here) that there are cancellations in the pressure; the contribution from the bonded interaction is negative, but this is compensated by the contribution from the nonbonded interactions. It is also seen that the contribution from the bonded interaction goes through minima when the density ρ reaches local maxima and vice versa, while the terms P_{inter} and P_{intra} follow the density profile (see Figure 7). Although these terms to a large extent cancel each other, they still reflect closely the structure of the density profile, and have large absolute values when the density is high. In Figure 8a we check that the pressure obtained in the bulk yields the same equation of state $p = p(\rho,T)$ irrespective of the value of the adsorption potential ϵ, as it should be: all data yield a single curve. The shape of this curve is similar to a corresponding calculation of bulk properties in a system with periodic boundary conditions throughout (no walls) done in previous work[51] at a slightly different temperature (full dots).

(b) Surface Tension. The pressure tensor $p_{\alpha\beta}(z)$ also is very useful for computing interfacial free energies.[59] Noting that in the center of the film ($z = D/2$) the normal component $p_N(z) \equiv p_{zz}(z)$ and the parallel (tranverse) component $p_T(z) \equiv (p_{xx}(z) + p_{yy}(z))/2$ are equal and hence there the system shows bulk behavior at the corresponding bulk density ρ_b, we can obtain interfacial tensions between the polymer solution at density ρ_b and the repulsive wall as well as the attractive wall as

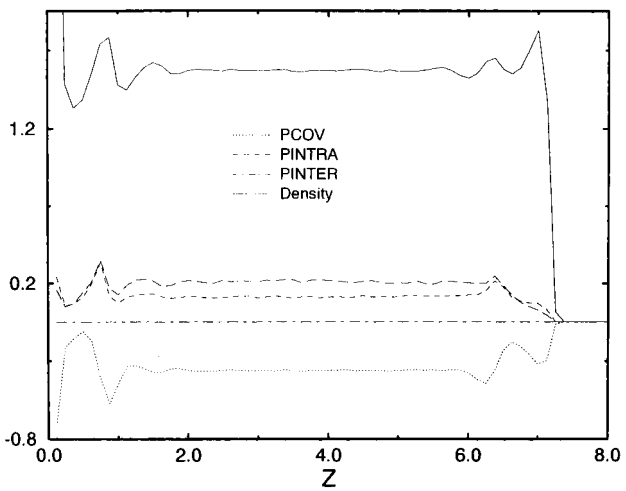

Figure 7. Comparison of the z component of the pressure with the density profile for the case $\epsilon = 2$, $\phi = 1.5$. The pressure is here split into individual contributions: p_{cov} is the contribution to the pressure from the bonded interaction (the FENE potential), which is negative; p_{intra} and p_{inter} are contributions from nonbonded interactions between monomers of the same chain and of different chains, respectively.

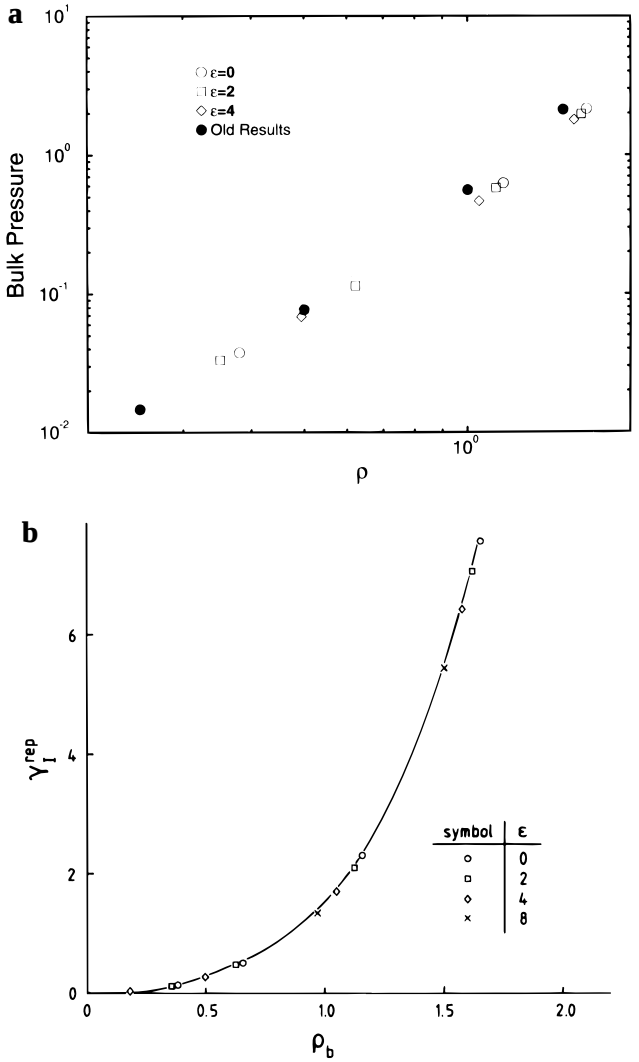

Figure 8. (a) Bulk pressure plotted versus bulk density ρ_b for three choices of ϵ (open symbols). Full dots show results of a previous study[51] of bulk properties carried out at a slightly higher temperature ($T = 1.2$). (b) Interfacial tension γ_I^{rep} between the polymer film and the repulsive wall plotted versus bulk density ρ_b for all four choices of ϵ. Curve is only drawn to guide the eye. Note that in our choice of units, where $T = 1$, $k_B = 1$, $\epsilon_M = 1$, and lengths are measured in units of $l_{max} = 1$, γ_I is dimensionless.

follows:[59]

$$\gamma_I^{rep} = \int_{D/2}^{D} dz\, [p_N(z) - p_T(z)]$$

$$\gamma_I^{attr} = \int_{0}^{D/2} dz\, [p_N(z) - p_T(z)] \qquad (12)$$

Here we are most interested in γ_I^{rep}, since this interfacial energy of the repulsive wall should be completely independent of the strength of the adsorption energy ϵ at the adsorbing wall; we expect γ_I^{rep} to be a function of the bulk density ρ_b only (and of temperature, of course, but we consider only $k_BT = 1.0$ here). Since the different choices of ϵ in our geometry with finite thickness do lead to different ρ_b, we get different results for $\gamma_I^{rep}(\phi)$ for the various choices of ϵ; but when we plot these results for γ_I^{rep} as function of ρ_b, all data should be part of a common curve. Figure 8b shows that this expectation is borne out very nicely, and this mutual consistency of our data proves the good accuracy of the applied procedures. As expected, γ_I^{rep} is a monotonically increasing function of density, and of order unity: it reflects the increasing energy cost of confining the chains in the film by the repulsive wall as ρ_b increases.

In contrast, γ_I^{attr} always stays much smaller and turns negative for the strongly adsorbing case ($\epsilon = 8$), indicating again that in this case spontaneous adsorption of the chains from the bulk of the film to the attractive wall occurs. Our data for γ_I^{attr} are also included in Table 1.

4. Dynamic Properties

Since the simulated system is both anisotropic and inhomogeneous, a precise characterization of the dynamics of the model is difficult—motions in directions parallel to the adsorbing wall will differ from motions in the perpendicular direction, and their character as well as their rate will depend on the transverse coordinates z of the monomers taking part in these motions. In our study, we did not attempt to unravel this complex behavior fully, but rather we are only concerned with an average description, where the inhomogeneity of motions is disregarded, and only the anisotropy is taken into account. In fact, anisotropy must not be ignored due to the confinement that the walls provide: so the diffusion constant $D_\perp$ in the perpendicular direction is clearly zero. Thus, we measure a corresponding perpendicular mean-square displacement of the center of gravity of the chains, $D_\perp^{eff}(t) = \langle [Z_{cm}(t) - Z_{cm}(0)]^2 \rangle / (2t)$, where $Z_{cm}(t)$ is the center of mass z coordinate of a chain at time t and $\langle ... \rangle$ means both an average over all chains and over the origin zero of time. We find that unlike $D_\parallel^{eff}(t) = \langle [X_{cm}(t) - X_{cm}(0)]^2 + [Y_{cm}(t) - Y_{cm}(0)]^2 \rangle / (4t)$ the effective diffusion constant $D_\perp^{eff}(t)$ does not settle down at a time-independent limit but continues to decrease steadily. Over time scales of $t \approx 10^5$ Monte Carlo steps (MCS), this decrease has been clearly found, at least for the lower densities ($\phi \leq 0.5$). From the plateau of $D_\parallel^{eff}(t)$ at large time, on the other hand, we are indeed able to estimate $D_\parallel$ as included in Table 1, where also relevant static quantities recorded in this study are included: bulk density ρ_b, interfacial tension γ_I^{attr}, and the parallel components of the gyration radius ($\langle R_g^2 \rangle_\parallel$) and the end-to-end distance ($\langle R^2 \rangle_\parallel$), respectively. In addition, we attempt to evaluate a relaxation time τ_R from the normalized autocorrelation function of the end-to-end vector,

$$\phi_R(t) = \langle \vec{R}(t) \cdot \vec{R}(0) \rangle / \langle R^2 \rangle \qquad (13)$$

fitting the decay at later times to an exponential function,

$$\phi_R(t) \approx \hat{\phi}_R \exp(-t/\rho_R), \qquad \text{large } t \qquad (14)$$

Figure 9 shows, as an illustration, that in typical case $\phi_R(t)$ follows eq 14 for $t > 10^3$ MCS already, and since the decay can be followed over one and a half decades, τ_R can be estimated with an accuracy of a few percent in this case.

It is important to note, however, that τ_R is the largest single-chain relaxation time, but not the largest collective relaxation time in our system, and *it is the largest collective relaxation time that controls equilibration of our system*. Noting from Table 1 that diffusion constants are of the order of 10^{-4} (note that in our units of length [$l_{max} = 1$] and time [one Monte Carlo step per monomer = 1] $D_\parallel$ is dimensionless), we can estimate the time τ_{coll} it takes to transport a chain from the vicinity of one wall to the other,

Table 1. Bulk Density ρ_b, Parallel Part of Mean-Square Gyration Radius $\langle R_g^2\rangle_{||}$ Averaged over the Film, Parallel Part of Mean-Square End-to-End Distance $\langle R^2\rangle_{||}$ Averaged Over the Film, Interfacial Tension between the Film and the Attractive Wall, γ_1^{attr}, and Diffusion Constant $D_{||}$ in the *x* and *y* Directions Averaged over the Film[a]

$\phi = 0.25$						$\phi = 0.50$					
ϵ	ρ_b	$\langle R_g^2\rangle_{||}$	$\langle R^2\rangle_{||}$	$D_{||}$	γ_1^{attr}	ϵ	ρ_b	$\langle R_g^2\rangle_{||}$	$\langle R^2\rangle_{||}$	$D_{||}$	γ_1^{attr}
0	0.382	4.25	27	2.3×10^{-4}	0.017	0	0.653	4.1	26	1.5×10^{-4}	0.037
2	0.356	4.28	27	2.5×10^{-4}	0.034	2	0.623	4.1	26	1.7×10^{-4}	0.076
4	0.178	5.17	33	1.4×10^{-4}	0.379	4	493	4.48	28	1.5×10^{-4}	0.409
8	0.069	5.49	30	3.0×10^{-5}		8	0.417				
$\phi = 1.00$						$\phi = 1.50$					
ϵ	ρ_b	$\langle R_g^2\rangle_{||}$	$\langle R^2\rangle_{||}$	$D_{||}$	γ_1^{attr}	ϵ	ρ_b	$\langle R_g^2\rangle_{||}$	$\langle R^2\rangle_{||}$	$D_{||}$	γ_1^{attr}
0	1.163	3.64	22	7.3×10^{-5}	0.079	0	1.652	3.39	21	2.4×10^{-5}	0.084
2	1.124	3.71	23	7.6×10^{-5}	0.187	2	1.621	3.44	21	2.4×10^{-5}	0.243
4	1.050	3.82	23	7.2×10^{-5}	0.432	4	1.575	3.41	21	2.4×10^{-5}	0.360
8	0.976	3.66	24	6.8×10^{-5}	−0.423	8	1.506	3.66	22	2.4×10^{-5}	−0.946

[a] All data are for a system size $32 \times 32 \times 8$ and chain length $N = 32$ at temperature $k_BT = 1$.

$$D^2 = 2D_{||}\tau_{coll} \Rightarrow \tau_{coll} = 3.2 \times 10^5 \qquad (15)$$

It is this time τ_{coll} which prevents us from studying significantly larger film thickness D, although this clearly would be desirable for small ϕ, where no bulk density and pressure could be reached in the center of the film (section 3).

Unfortunately, for both larger density and larger ϵ the decay of $\ln \phi_R(t)$ vs t is rather curved, and in addition there are fairly strong statistical fluctuations. These problems precluded us from obtaining reliable estimates of the relaxation time τ_R in these cases.

More detailed information on the dynamics of the individual monomers and chains is obtained by following appropriate mean-square displacements with time. We have studied the following quantities,[40,41,49,60] denoting the xy coordinates of a monomer i as $\vec{\rho}_i$ and the xy coordinates of the center of mass as $\vec{\rho}_{cm}$,

$$g_{1xy}(t) = \langle[\vec{\rho}_i(t) - \vec{\rho}_i(0)]^2\rangle \qquad (16)$$

$$g_{1z}(t) = \langle[z_i(t) - z_i(0)]^2\rangle \qquad (17)$$

$$g_{2xy}(t) = \langle[\vec{\rho}_i(t) - \vec{\rho}_{cm}(t) - \vec{\rho}(0) + \vec{\rho}_{cm}(0)]^2\rangle \qquad (18)$$

$$g_{2z}(t) = \langle[z_i(t) - z_{cm}(t) - z_i(0) + z_{cm}(0)]^2\rangle \qquad (19)$$

$$g_{3xy}(t) = \langle[\vec{\rho}_{cm}(t) - \vec{\rho}_{cm}(0)]^2\rangle \qquad (20)$$

$$g_{3z}(t) = \langle[z_{cm}(t) - z_{cm}(0)^2]\rangle \qquad (21)$$

Again here an average is taken over all inner monomers of all chains to compute eqs 16−19, irrespective of whether the chains are adsorbed at the wall or belong to the neighboring solution. In addition, an average is taken over the time origin from which on the displacements are studied in the simulation.

Figure 10 shows typical data, confining attention to the nonadsorbed ($\epsilon = 2$) cases and low densities ($\phi = 0.25$, 0.50). The behavior of these displacements is similar to what one sees in a bulk dilute ($\phi = 0.25$) or semidilute ($\phi = 0.50$) solution, with a few significant differences: the displacement $g_{3z}(t)$ initially is smaller than $g_{3xy}(t)$ by a factor of 2 (which trivially follows from the definition of $g_{3xy}(t)$, to which two coordinates x,y rather than a single one contribute), but at large time this difference increases, since only g_{3xy} continues to increase linearly with time, while $g_{3z}(t)$ bends over to reach a finite saturation value, as it must due to the confinement caused by the walls. The time where this happens corroborates our estimate, eq 15. Also the displacements $g_{1z}(t)$ and $g_{2z}(t)$ bend over to constant saturation values. Of course, the displacements of inner monomers measured in the center of mass system of a chain $\{g_{2z}(t), g_{2xy}(t)\}$ always saturate, since a monomer cannot diffuse arbitrarily far away from the center of the mass of the chain to which it belongs, but only distances of the order of $\langle R_g^2\rangle^{1/2}$. This saturation of $g_{2z}(t)$, $g_{2xy}(t)$ occurs on the (shorter) time scale τ_R, and consequently we see from Figure 10b (where τ_R, τ_{coll} are appreciably different) that $g_{2z}(t)$, $g_{2xy}(t)$ at times of order 10^4 are nearly completely saturated, while $g_{1z}(t)$, $g_{3z}(t)$ still increase and saturate at the later time τ_{coll} (eq 15). The mean-square displacements $g_{1xy}(t)$, $g_{3xy}(t)$ are close to their expected behaviors,[61]

$$g_{1xy}(t) \propto t^{1/(1+/2\nu)} \approx t^{0.54} \qquad g_{3xy}(t) \propto t \qquad (22)$$

Here we have taken the three-dimensional exponent $\nu \approx 0.59$ and not the two-dimensional one ($\nu = {}^3/_4$), since the chains are not yet strongly adsorbed for $\epsilon = 2$, and so the behavior is dominated by that of dilute solutions. Actually, the effective exponents extracted from best fits to the data shown in Figure 9 are slightly different, namely $g_{1xy}(t) \propto t^{0.62}$ and $g_{3xy}(t) \propto t^{0.97}$. Such discrepancies have also been observed in another context,[40,41,49] where it was shown that these discrepancies are due to the shortness of the chains that were studied and disappear gradually when one studies longer and longer chains.

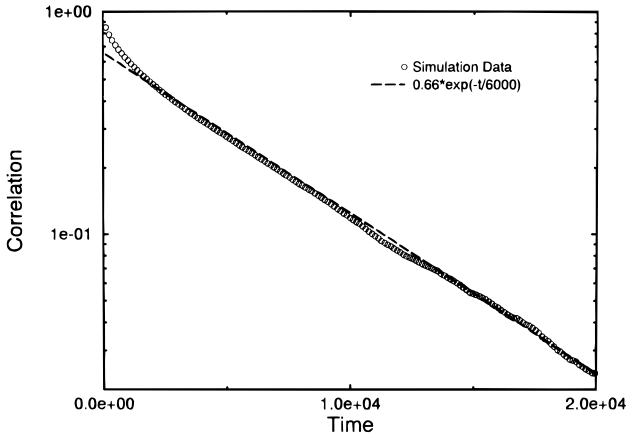

Figure 9. Semilogarithmic plot of the end-to-end vector autocorrelation function $\phi_R(t)$ versus time t for $\epsilon = 2$ and $\phi = 0.25$. Open circles show the simulation data, and the broken straight line the fit to eq 13.

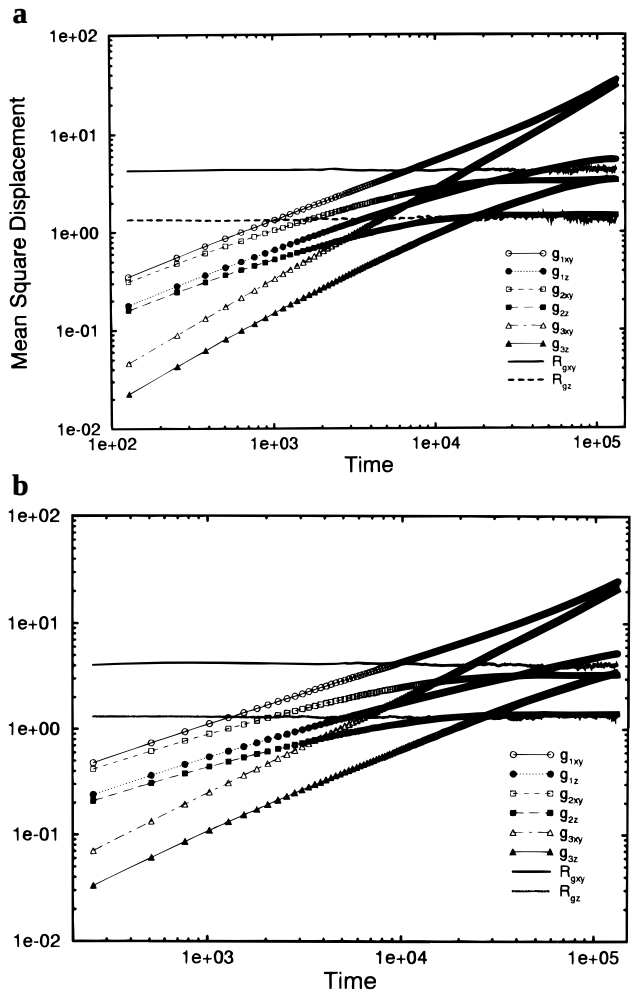

Figure 10. log−log plot of mean-square displacements $g_{1xy}(t)$, $g_{1z}(t)$, $g_{2xy}(t)$, $g_{2z}(t)$, $g_{3xy}(t)$, $g_{3z}(t)$ versus time. Also the corresponding components of the mean-square gyration radius (denoted as R_{gxy}, R_{gz}) are included. Cases shown are $\epsilon = 2$, $\phi = 0.25$ (a) and $\epsilon = 2$, $\phi = 0.50$ (b). Cases $\epsilon = 0$, $\phi = 0.25$ and $\epsilon = 0$, $\phi = 0.50$ are almost identical to cases a and b and hence are not shown here.

5. Conclusions

In this paper we have studied the equilibrium between one adsorbing wall and an adjacent polymer solution, varying both the strength ϵ of the (short range) adsorption potential and the density of the solution, but restricting attention to the good solvent case ($T = 1$, exceeding distinctly the theta temperature $\Theta = 0.62$) and studying a single, rather short, chain length only ($N = 32$). It was shown that under these conditions one gets for large ϵ ($\epsilon \geq 4$) a dense monolayer at the adsorbing wall, which then also produces pronounced oscillations in the density profile, in particular for semidilute and concentrated polymer solutions. However, the surface excess density caused by the adsorption potential stays of order unity throughout; i.e., the adsorbed amount of polymer is due to the excess of one or two dense polymeric layers at the wall only. One does not obtain a situation where an adsorbed thick film coexists with an adjacent dilute solution, unlike the situation possible for $T < \Theta$, which will be studied elsewhere.

We have also shown that recording the profile of the pressure tensor components P_x, P_y, and P_z is very useful to judge the quality of the equilibrium that has been achieved and for the distinction where bulk behavior begins and the pressure tensor is isotropic ($P_x = P_y = P_z$) from the region of the adsorbed surface layer where it is anisotropic. The relation between pressure and density in such inhomogeneous situations should also yield useful information on the equation of state of the considered model system. It is shown that also interfacial tensions between the polymer film and both the attractive and the repulsive wall can be extracted. With regard to dynamic properties, it is conceptually difficult to disentangle contributions due to monomers bound to the wall from contributions of monomers in the adjacent polymer solution. We have thus averaged the behavior of mean-square displacements, relaxation times, etc. over the region throughout the whole film. However, the behavior then is not very different from corresponding bulk systems with no adsorbing walls at all. Clearly, more work will be required for properly isolating the effects that chains bound to the attractive wall have on dynamic properties of thin polymeric films.

Acknowledgment. This work was supported by the Deutsche Forschungsgemeinschaft (DFG) under Grants SFB 262/D2 and 435BUL-113/45. A.M. gratefully acknowledges support from the Bulgarian National Foundation for Scientific Research under Grant X-301. R.B.P. enjoyed the warm hospitality during his visit at the Johannes Gutenberg Universität Mainz.

References and Notes

(1) Wu, S. *Polymer Interfaces and Adhesion*; Marcel Dekker: New York, 1982.
(2) Cohen-Stuart, M. A.; Cosgrove, T.; Vincent, B. *Adv. Colloid Interface Sci.* **1986**, *24*, *143.*
(3) de Gennes, P. G. *Adv. Colloid Interface Sci.* **1987**, *27*, 189.
(4) Koberstein, J. T. In *Encyclopedia of Polymer Science and Engineering*; Mark, H., Overberger, C. G., Bikales, N. M., Menges, G., Eds.; Wiley: New York, 1987; Vol. 8, p 237.
(5) Russell, T. P. *Annu. Rev. Mater. Sci.* **1991**, *21*, 249.
(6) Stamm, M. *Adv. Polym. Sci.* **1992**, *100*, 357.
(7) Sanchez, I. C., Ed. *Physics of Polymer Surfaces and Interfaces*; Butterworth-Heinemann: Boston, 1992.
(8) Halperin, A.; Tirrell, M.; Lodge, T. P. *Adv. Polym. Sci.* **1992**, *100*, 31.
(9) Eisenriegler, E. *Polymers near Surfaces*; World Scientific: Singapore, 1993.
(10) Tirrell, M.; Parsonage, E. E. In *Structure and Properties of Polymers*; Thomas, E. L., Ed.; VCH Verlagsges.: Weinheim, 1993; p 653.
(11) Fleer, G. J.; Cohen-Stuart, M. A.; Scheutjens, J. M. H.; Cosgrove, T.; Vincent, B. *Polymers at Interfaces*; Chapman and Hall: London, 1993.
(12) Binder, K. *Acta Polym.* **1995**, *46*, 204.
(13) de Gennes, P. G. In *Molecular Conformation and Dynamics of Macromolecules in Condensed Systems*; Nagasawa, M., Ed.; Elsevier: Amsterdam, 1988; p 315.
(14) Léger, L.; Hervet, H.; Silberzan, P.; Frot, D. In *Dynamical Phenomena at Interfaces, Surfaces and Membranes*; Beysens, D., Boccara, N., Forgacs, G., Eds.; Nova Science Publ.: Commack, 1993; p 499. Frantz, P. J.; Granick, S. *Phys. Rev. Lett.* **1991**, *66*, 899.
(15) For a recent review, see: Yoon, D. Y.; Vacatello, M.; Smith, G. D. In *Monte Carlo Molecular Dynamics Simulations in Polymer Science*; Binder, K., Ed.; Oxford University Press: New York, 1995; p 433.
(16) Dickman, R.; Hall, C. K. *J. Chem. Phys.* **1988**, *89*, 3168.
(17) Kumar, S. K.; Vacatello, M.; Yoon, D. Y. *J. Chem. Phys.* **1988**, *89*, 5206.
(18) Kumar, S. K.; Vacatello, M.; Yoon, D. Y. *Macromolecules* **1990**, 23, 2189.
(19) Bitsanis, I. A.; Hadziioannou, G. *J. Chem. Phys.* **1990**, *92*, 3827.
(20) Yethiraj, A.; Hall, C. K. *Macromolecules* **1990**, *23*, 1865.
(21) Wang, J.-S.; Binder, K. *J. Phys. I (Fr.)* **1991**, *1*, 1583.
(22) Mansfield, K. F.; Theodorou, D. N. *Macromolecules* **1991**, *24*, 6283.
(23) Thompson, P. A.; Grest, G. S.; Robbins, M. O. *Phys. Rev. Lett.* **1992**, *68*, 3448.

(24) Xia, T. K.; Ouyang, J.; Ribarsky, M. W.; Landman, U. *Phys. Rev. Lett.* **1992**, *69*, 1967.
(25) Bitsanis, I. A.; ten Brinke, G. *J. Chem. Phys.* **1993**, *99*, 3100.
(26) Manias, E.; Hadziioannou, G.; Bitsanis, I. A.; ten Brinke, G. *Europhys. Lett.* **1993**, *24*, 99.
(27) Bitsanis, I. A.; Pan, C. *J. Chem. Phys.* **1993**, *99*, 5520.
(28) Winkler, R. G.; Matsuda, T.; Yoon, D. Y. *J. Chem. Phys.* **1993**, *98*, 729.
(29) Yethiraj, A. *J. Chem. Phys.* **1994**, *101*, 2489.
(30) Milchev, A.; Paul, W.; Binder, K. *Macromol. Theory Simul.* **1994**, *3*, 305.
(31) Manias, E.; Hadziioannou, G.; ten Brinke, G. *J. Chem. Phys.* **1994**, *101*, 1721.
(32) Gupta, S.; Koopman, D. C.; Westermann-Clark, G. B.; Bitsanis, I. A. *J. Chem. Phys.* **1994**, *100*, 8444.
(33) Hariharan, A.; Harris, J. G. *J. Chem. Phys.* **1994**, *101*, 4156.
(34) Matsuda, T.; Smith, G. D.; Winkler, R. G.; Yoon, D. Y. *Macromolecules* 1995, *28*, 165.
(35) Subbotin, A.; Semenov, A.; Manias, E.; Hadziioannou, G.; ten Brinke, G. *Macromolecules* **1995**, *28*, 1511.
(36) Subbotin, A.; Semenov, A.; Hadziioannou, G.; ten Brinke, G. *Macromolecules* **1995**, *28*, 3901.
(37) Manias, E.; Subbotin, A.; Hadziioannou, G.; ten Brinke, G. *Mol. Phys.* **1995**, *85*, 1017.
(38) Baschnagel, J.; Binder, K. *Macromolecules* **1995**, *28*, 6808. Baschnagel, J.; Binder, K. *J. Phys. II (Fr.)* **1996**, *6*, 1271.
(39) Lai, P.-Y. *J. Chem. Phys.* **1995**, *103*, 5742; *Macromol. Theory Simul.* **1996**, *5*, 255.
(40) Milchev, A.; Binder, K. *Macromolecules* **1996**, *29*, 343.
(41) Milchev, A.; Binder, K. *J. Phys. II (Fr.)* **1996**, *6*, 21.
(42) Milchev, A.; Binder, K. *J. Computer-Aided Mater. Des.* **1996**, *2*, 167.
(43) Binder, K.; Milchev, A.; Baschnagel, J. *Annu. Rev. Mater. Sci.* **1996**, *26*, 107.
(44) Zajac, R.; Chakrabarti, A. *J. Chem. Phys.* **1996**, *104*, 2418.
(45) Binder, K. *Makromol. Chem., Macromol. Symp.* **1991**, *50*, 1.
(46) Binder, K. In *Computational Modeling of Polymers*; Bicerano, J., Ed.; Marcel Dekker: New York, 1992; p 221.
(47) Binder K. In *Monte Carlo and Molecular Dynamics Simulations in Polymer Science*; Binder, K., Ed.; Oxford University Press: New York, 1995; p 3.
(48) Leontidis, E.; Forrest, B. M.; Widmann, A. H.; Suter, U. W. *J. Chem. Soc., Faraday Trans.* **1995**, *91*, 2355.
(49) Milchev, A.; Paul.;W.; Binder, K. *J. Chem. Phys.* **1993**, *99*, 4786.
(50) Gerroff, I.; Milchev, A.; Binder, K.; Paul, W. *J. Chem. Phys.* **1993**, *98*, 6526.
(51) Milchev, A.; Binder, K. *Macromol. Theory Simul.* **1994**, *3*, 915.
(52) Milchev, A.; Binder, K. *Europhys. Lett.* **1994**, *26*, 671.
(53) de Gennes, P. G. *Scaling Concepts in Polymer Physics*; Cornell University Press: Ithaca, NY, 1979.
(54) Doi, M.; Edwards, S. F. *The Theory of Polymer Dynamics*; Clarendon Press: Oxford, 1986.
(55) de Gennes, P. G. *Macromolecules* **1981**, *14*, 1637.
(56) Eisenriegler, E.; Kremer, K.; Binder, K. *J. Chem. Phys.* **1982**, *77*, 6296.
(57) Yamakov, V.; Milchev, A.; Binder, K., in preparation.
(58) Allen, M. Tildesley, D. J. *Computer Simulation of Liquids*; Clarendon: Oxford, 1987.
(59) Smit, B. *Phys. Rev. A* **1988**, 37, 3481. Alegandre, J.; Tildesley, D. J.; Chapela, G. A. *J. Chem. Phys.* **1995**, *102*, 4574; *Mol. Phys.* **1995**, *85*, 651.
(60) Paul, W.; Binder, K.; Heermann, D. W.; Kremer, K. *J. Chem. Phys.* **1991**, *95*, 7726.
(61) Kremer, K.; Binder, K. *J. Chem. Phys.* **1984**, *81*, 6381.

MA961342L